NANO LETTERS

pubs.acs.org/NanoLett Letter

Single-Shot Multispectral Encoding: Advancing Optical Lithography for Encryption and Spectroscopy

Hyewon Shim, Geonwoong Park, Hyunsuk Yun, Sunmin Ryu, Yong-Young Noh,* and Cheol-Joo Kim*

Cite This: https://doi.org/10.1021/acs.nanolett.4c02153 Read Online

ACCESS | Metrics & More | Article Recommendations | Supporting Information

ABSTRACT: Most modern optical display and sensing devices utilize a limited number of spectral units within the visible range, based on human color perception. In contrast, the rapid advancement of machine-based pattern recognition and spectral analysis could facilitate the use of multispectral functional units, yet the challenge of creating complex, high-definition, and reproducible patterns with an increasing number of spectral units limits their widespread application. Here, we report a technique for optical lithography that employs a single-shot exposure to reproduce perovskite films with spatially controlled optical band gaps through light-induced compositional modulations. Luminescent patterns are designed to program correlations between spatial and spectral information, covering the entire visible spectral range. Using this platform, we demonstrate multispectral encoding patterns for encryption and multivariate optical converters for dispersive optics-free spectroscopy with high spectral resolution. The fabrication process is conducted at room temperature and can be extended to other material and device platforms.

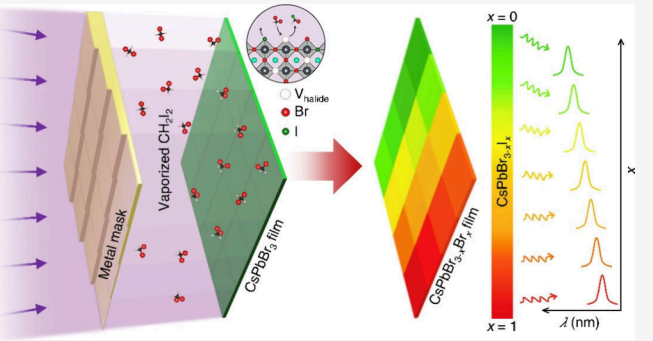

KEYWORDS: *multispectral optical element, optical lithography, luminescent pattern, compressive spectroscopy, optical encryption, semiconductor alloy pattern*

Optical sensors and displays play key roles in capturing and transporting optical information in modern information technology. As the number of units with varying spectral responses increases in devices, so too does the potential for multiplexed optical information within a broad bandwidth. However, the majority of devices are designed based on the trichromatic red-green-blue (RGB) color scheme, optimized for human color perceptions.[1] Recently, with the prevalence of machine-based analyses of optical patterns in both spatial and spectral domains, there is a significant demand for a multispectral optical platform.[2,3] This platform functions in two main roles: (*I*) transforming spectral information into spatially programmed patterns, and (*II*) translating geometric information into specific emissive spectra with programmed correlations between the spatial coordinates of the optical element and the optical spectra after light-matter interactions, as depicted in Figure 1A. These capabilities enable the development of advanced optical and optoelectronic device applications, including multiplexing in optical communications,[4,5] broadband displays exceeding the red-green-blue color model,[6,7] and compact spectral analysis tools.[8−10]

To manipulate the light spectrum across a broad band region through light-matter interactions, semiconductor alloys provide a compact, solid-state platform with continuously variable energy band gaps as their compositions change[11] (Figure 1A). These alloys not only exhibit a broad spectrum range but can also be integrated within the same material platform to realize multispectral systems. Methods for both step-by-step[12,13] and simultaneous integrations[14,15] of alloys have been developed. However, spatially controlled integration becomes increasingly challenging as the number of spectral units required to extend multispectral bandwidth increases. Consequently, many promising ideas for multispectral functional elements remain at the proof-of-concept stage due to reproducibility challenges in fabricating identical structural copies through multiple integration processes. This often necessitates a fine calibration step after each fabrication to achieve the required optical properties on demand.

Here, we present a single-shot optical lithography technique for creating multispectral patterns in semiconductor alloys (Figure 1B). Uniform semiconducting $CsPbBr_3$ perovskite films were deposited on substrates via solution processes at room temperature[16] (see Figure S2 for the film's characterization data). Single-shot optical lithography was performed on

Received: May 8, 2024
Revised: August 23, 2024
Accepted: August 26, 2024

https://doi.org/10.1021/acs.nanolett.4c02153
Nano Lett. XXXX, XXX, XXX−XXX

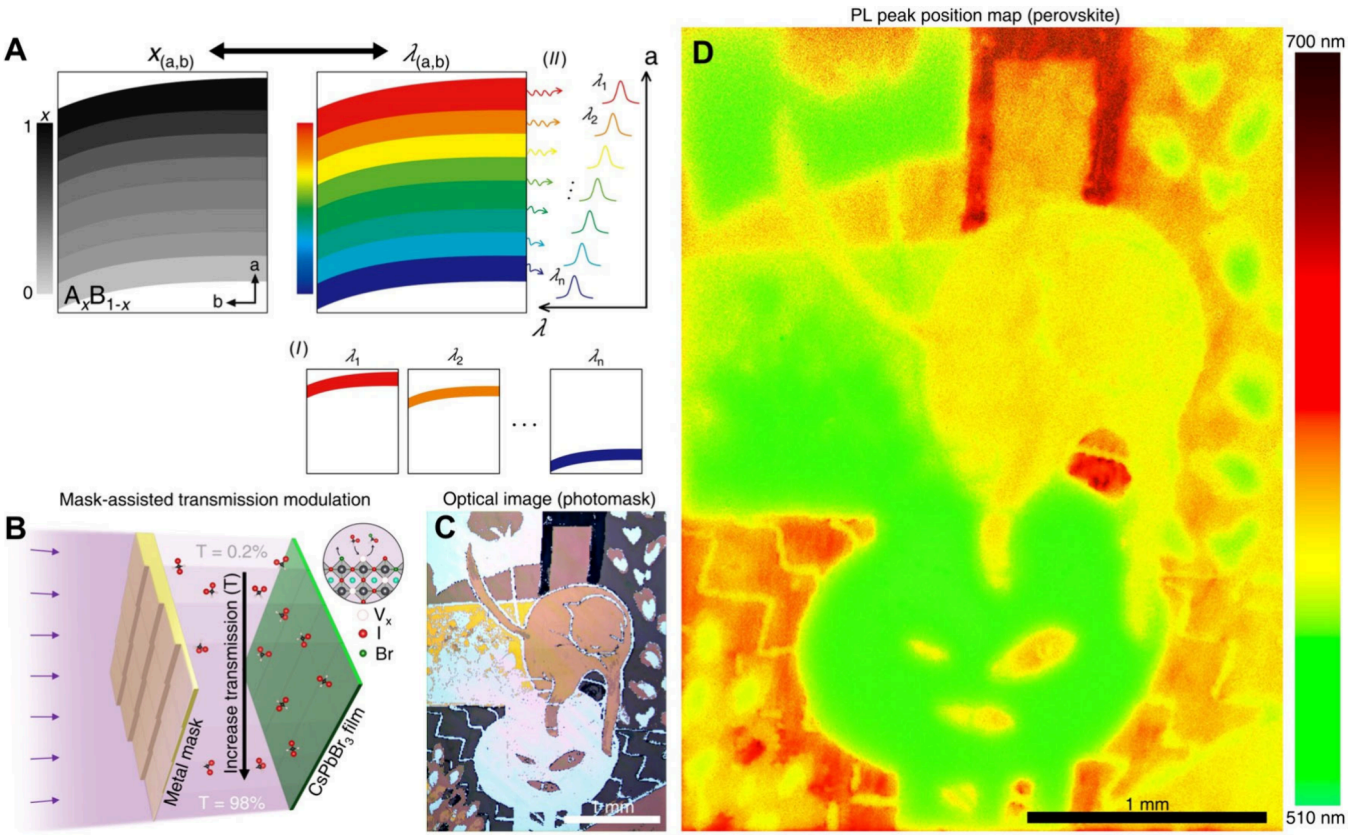

Figure 1. Single-shot Optical Lithography for Multispectral Patterns. (A) Schematics for a multispectral optical platform with programmed correlations between semiconductor alloy composition and optical spectra. (B) Illustration of single-shot optical lithography process for multispectral patterning with optical density-graded photomask. (C) Optical reflectance image of a photomask, replicating a drawing of a cat with fishes. (D) PL peak position map of $CsPbI_xBr_{3-x}$ perovskite film after multispectral patterning.

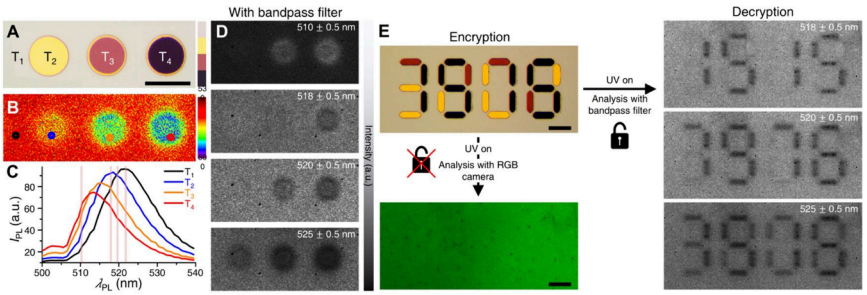

Figure 2. Multispectral Optical Encryption. (A) Optical reflectance image of a density-graded photomask. Scale bar: 50 μm. (B) PL peak position map of patterned $CsPbCl_xBr_{3-x}$ perovskite, using the photomask shown in (A). (C) Local PL spectra corresponding to the circled areas in (B). (D) Fluorescence images captured with bandpass filters, whose bandwidths are shown in (C) with shadowed pink vertical lines. (E) Optical encryption of numeric codes patterned in perovskite. The bottom-left image is the fluorescent image under UV illumination, taken with a conventional RGB sensor. The right images show wavelength-dependent PL images through bandpass filters with different bandwidths, indicated at the right top corners.

the film by illuminating it with the light of approximately 405 nm through a photomask in a controlled environment with vapor-phase precursors of dihalomethane (CH_2X_2, X = Cl, Br, I) in a custom-built chamber (Figure S1). A predesigned metal mask with spatially varying thicknesses was used to modulate local light transmission from 0% to nearly 100% (Figure S3A), forming alloy patterns directly through controlled anion exchanges facilitated by the photoinduced decomposition of CH_2X_2,[17,18] without the use of photoresist. This process allows numerous different alloy compositions to be simultaneously achieved in a single step at the desired locations, resulting in multispectral patterns with high spectral resolution and reproducibility.

Utilizing the designed optical density-modulated photomask (Figure 1C), we have fabricated a multispectral fluorescent pattern that replicates a drawing of a cat with fishes on $CsPbBr_{3-x}I_x$ films. This was achieved where photoinduced decomposition of CH_2I_2 occurred in $CsPbBr_3$ films. The photoluminescence (PL) peak wavelength, λ_{PL} mapping data (Figure 1D), reveals the targeted features, thereby demonstrating the conversion of the optical density pattern into a spectral pattern. The multiple converted regions display programmed λ_{PL}, spanning from 523 to 606 nm, corresponding to the

https://doi.org/10.1021/acs.nanolett.4c02153
Nano Lett. XXXX, XXX, XXX−XXX

original $CsPbBr_3$ and $CsPbBr_{1.4}I_{1.6}$, respectively. Local PL spectra (Figure S3B,C), taken from various regions, exhibit singular PL peaks, indicating that homogeneous $CsPbBr_{3-x}I_x$ alloys without phase segregation have formed across the entire spectrum range, maintaining the direct bandgap nature.[19] Notably, no halogen exchange occurred without incident light, as evidenced by the identical λ_{PL} after the process compared to the original $CsPbBr_3$ (Figure S2D). We also confirmed that the pattern could be replicated by repeating the process with the same multispectral mask (Figure S3D). While several reports[20,21] have discussed local composition modulations of perovskite alloys through postsynthetic anion exchanges, the number of possible spectral units was often limited due to integration issues, precluding the fabrication of large-scale multispectral patterns with high definition.

The material design platform is versatile, suitable for designing multiband components that fulfill the two key functions described in Figure 1A. To demonstrate function (*I*), we exhibit pattern encryptions, where λ_{PL}-dependent spatial patterns are encoded with precise spectral modulations. In Figure 2A–C, the λ_{PL} from local regions of the $CsPbBr_3$ film is slightly altered by controlling the incorporation of chloride elements with different gaseous precursors (see Methods), using the same lithography process with an optical density-graded photomask. Each programmed area displays a different PL spectrum with subtly tuned λ_{PL} within 10 nm intervals (Figure 2C). Selecting a certain bandwidth of PL (indicated by vertical shadowed pink lines in Figure 2C) with bandpass filters, the relative PL intensity, I_{PL}, from different regions changes, creating bandwidth-dependent fluorescent intensity patterns, as shown in Figure 2D. Employing this mechanism, we patterned multiplexed fluorescent patterns of numeric codes in a $CsPbBr_{3-x}Cl_x$ perovskite film (Figure 2E). Given that the spectral modulation is precisely conducted within a narrow bandwidth, it is difficult for conventional sensor and display units with Bayer filters to capture and reproduce the fluorescent patterns (Figure 2E, bottom left). However, when bandpass filters with narrow 1 nm bandwidths are used at different center wavelengths, wavelength-dependent numeric codes become visible as "1515" at 518 nm, "7976" at 520 nm, and "3808" at 525 nm. This demonstrates that multiple λ_{PL}-dependent patterns can be employed to thwart decryption attempts by incorporating numerous false patterns.

As the spectra are determined by the intrinsic optical band gaps of semiconductors, the λ_{PL} can be tuned within a desired wavelength range to form patterns of arbitrary shapes and sizes in the macroscopic regime. To demonstrate the versatility of our process, we patterned a QR code linking to the web page of our laboratory by slightly modulating the PL spectra in $CsPbI_xBr_{3-x}$ perovskite films. The binary pattern is constructed using two spectral units with slightly different λ_{PL} of 545 and 557 nm, respectively (Figure 3A), with a central wavelength peak of approximately 550 nm, emitting yellow fluorescent light (Figure 3B). Hue purity discrimination by color perception is known to be weakest for yellow light against a white background for the majority of people, as the most sensitive M- and L-cone cells are similarly activated by both yellow and white light.[22] Therefore, it is challenging to recognize the pattern with the naked eye or conventional sensors with Bayer filters, and the designed pattern was revealed in high contrast only when the correct spectral filter was applied (Figure 3C). We note that the PL spectra are maintained regardless of the viewing angle or light source,

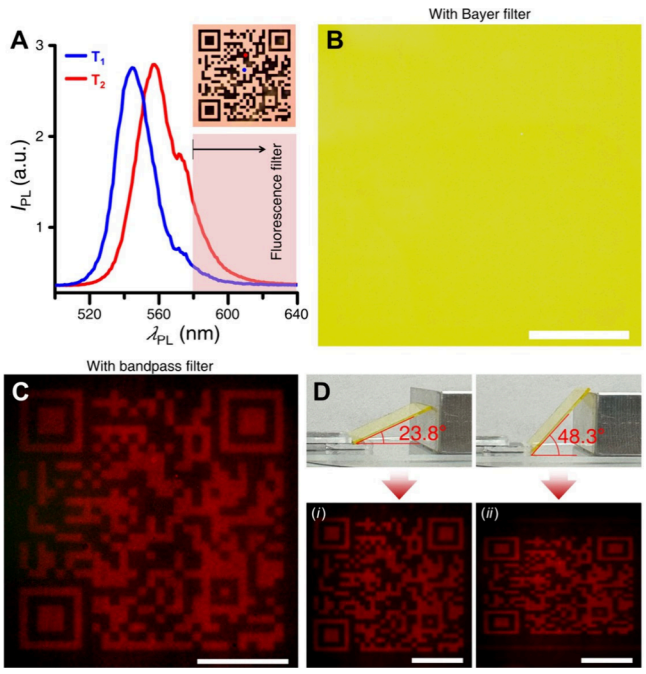

Figure 3. Encrypted PL Patterns with Tunable Center Wavelengths. (A) PL spectra from binary $CsPbI_xBr_{3-x}$ patterns of a QR code (inset). The shadowed area indicates the transmitted range of the long-pass filter used in (C) and (D). The central wavelength peak, determined by the intrinsic optical band gap, is approximately 550 nm, emitting yellow fluorescent light. (B) Fluorescence image of the patterned perovskite, taken by an image sensor with a Bayer filter. (C) Fluorescence image of the same film through the long-pass filter. (D) (top) Photographs of the film at different tilt angles, and (bottom) fluorescence images through the long-pass filter. The same pattern is maintained regardless of the viewing angle. All scale bars: 500 μm.

generating PL-dependent fluorescent patterns that are recognizable by image sensors (Figure 3D), unlike the case with spectral filters used to create structural colors.[23,24] These measurements confirm that encryption can be achieved on surfaces with curvature, such as flexible substrates, for a broad range of applications.[25,26] The pattern can be maintained for several months, demonstrating the long retention time, despite of intermixing between two phases in the binary pattern (Figure S5). Also, the pattern can be erased for writing a new pattern in the same film (Figure S6).

Our encryption approach offers several significant advantages over previous methods.[27−31] First, cryptographic security is enhanced because the optical information can only be decoded by selecting the appropriate filter bandwidth. Material systems for optical encryption are generally fabricated by patterning a specific chemical substance, designed to provide optical contrast with the surroundings and reveal hidden patterns when subjected to targeted external stimuli, such as temperature changes,[27,28] moisture,[29] and chemical reactions with solvents.[30,32] However, the responsiveness of the patterned chemicals can sometimes exhibit poor selectivity to these stimuli. For instance, the optical properties of molecules are frequently influenced by interactions with various molecules, which increases the risk of information leakage through unauthorized decryption attempts. In contrast, our method encodes patterns through subtle changes in chemical composition, making them challenging to decipher without precise bandwidth information.

https://doi.org/10.1021/acs.nanolett.4c02153
Nano Lett. XXXX, XXX, XXX−XXX

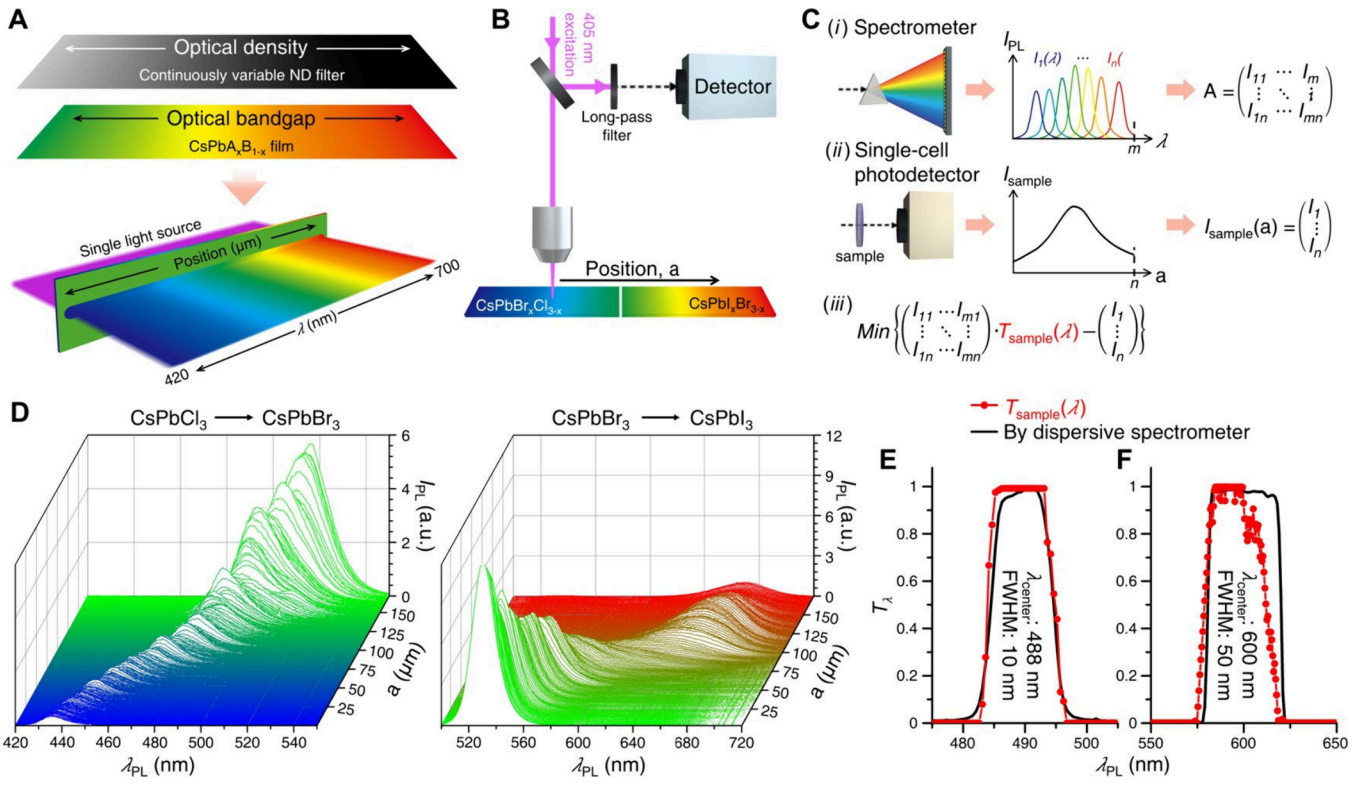

Figure 4. Compressive Optical Spectroscopy with Multispectral Emission Films. (A) Schematic of a multispectral emission film, fabricated by translating optical density information into spectral information. The emission spectra from a single light source are tuned by manipulating the spatial coordinates. (B) Schematic of a miniaturized spectrometer. (C) The operations of compressive spectroscopy. (D) Position-dependent local PL spectra of $CsPbBr_xCl_{3-x}$ and $CsPbI_xBr_{3-x}$. (E) and (F) is two bandpass filters with different bandwidths are used as the reference samples, whose transmittance data are shown in black. The deduced $T_{sample}(\lambda)$ by the compressive optical spectroscopy is shown in red.

In addition, decoding the fluorescent pattern is a nondestructive process, unlike invasive methods where the material platform undergoes chemical or structural change to become optically active.[28−30] Consequently, our films are suitable for the development of optoelectronic devices capable of dynamically generating various encryption patterns on a single platform. For example, an array of green-light emitting diodes could be created, each with slight spectral shifts that are only detectable using the correct bandpass filters. Given the heightened risk of image information exposure due to the prevalent use of electromagnetic wave sensors in contemporary society,[32] this platform offers a promising avenue for enhancing security in optoelectronic devices beyond the traditional red/green/blue color scheme.

We now demonstrate Function (*II*) of the programmable multispectral emissive elements, which tune emission spectra by manipulating the coordinates defining the PL emission area (Figure 4A). Whereas monochromators and interferometers achieve the same functionality by utilizing moving optical elements, such as gratings and mirrors, to select the desired band from a broadband light source, our method generates multivariant PL spectra through the down-conversion of single-wavelength excitation light at each position. Consequently, this multivariant optical film can be paired with a continuous-wave laser, rather than bulky lamps, to create a wavelength-tunable light source for optical spectroscopy. Given that the excitation laser can be focused to diffraction limits, the emitted light from a small size sample can cover a broad spectral range. This is achieved by raster-scanning the confocal excitation over a compact film, wherein different semiconductor alloys are densely integrated, facilitating the realization of a miniaturized spectrometer (Figure 4B,C).

We fabricated continuous composition-graded $CsPbCl_{3-x}Br_x$ and $CsPbI_xBr_{3-x}$ alloy films with x values, ranging from 0 to nearly 3 along a fixed direction. A continuously variable optical density filter served as the photomask for multispectral lithography, enabling the translation of optical density information into spectral information (Figure 4A). The local PL spectra, obtained by a confocal microscope, exhibit single peaks with position-dependent λ_{PL}, spanning the entire visible spectral range (Figure 4D). This indicates the absence of abrupt changes in optical band gaps within the scanned area. In this process, all the spectral units are integrated within a narrowly defined region, only 175 μm wide, a feat challenging to accomplish using conventional step-by-step integration methods.[8,12,13,20]

This system serves as a dispersive optics-free spectrometer for optical characterizations. After characterizing the PL properties of the multivariant emissive film to obtain the three-dimensional plot of I_{PL} (Figure 4D), which can be represented by an m-by-n transfer matrix, A, with rows and columns corresponding to spatial and spectral coordinates respectively (Figure 4C), the position-dependent $I_{PL}(a)$ is measured through a sample of interest using a single-cell photodetector without a spectrometer. If $T_{sample}(\lambda)$ represents an n-by-1 matrix for the optical transmission of PL signals at each wavelength through the sample, then it can be deduced by optimization fitting to minimize $A \cdot T_{sample}(\lambda) - I_{sample}(a)$, where $I_{sample}(a)$ represents an m-by-1 matrix for the position-dependent I_{PL} (refer to the Supporting Information for a

https://doi.org/10.1021/acs.nanolett.4c02153
Nano Lett. XXXX, XXX, XXX−XXX

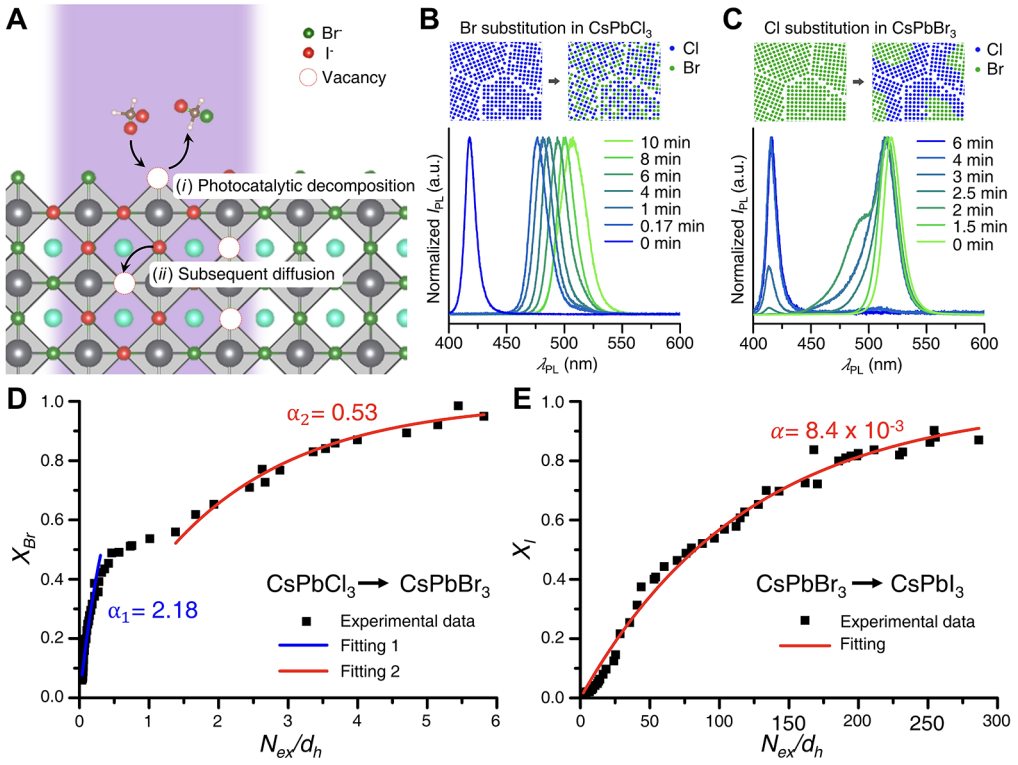

Figure 5. Kinetics for Photocatalytic Conversion of Halides in Semiconductor Alloys. (A) Schematic of the halide anion exchange process in perovskites. (B) and (C) is PL spectra with different reaction times for (D) Br replacement with Cl, starting from $CsPbCl_3$, and (C) Cl replacement with Br, starting from $CsPbBr_3$. (D) and (E) The composition ratio of the substituted halogen anion, X_H (H = Br or I), as a function of photoexcited carrier density, N_{ex}, normalized by the areal density of halogen elements at the surface, d_h. Solid lines represent the fitting based on an asymptotic exponential function representing saturated exchange behavior, where α indicates the photocatalytic efficiency for halogen exchanges.

detailed process). We used two narrow bandpass filters as reference samples to validate our approach and confirmed that the deduced $T_{sample}(\lambda)$ (red color spectra in Figure 4E,F) closely matches the transmission spectra measured with a conventional monochromator (black spectra). Notably, as m, the number of spectra with different λ_{PL} at various positions can exceed n, the number of spectral values, which is limited by the spectral resolution of the spectrometer used to acquire A, one can maintain high spectral resolution to detect the narrow bandwidth of the references through the optimization process.

Our approach to design multispectral patterns can be versatile to apply to different semiconductor alloy systems with right selections of the host film and gaseous precursor. The exchange process primarily consists of two steps: (*i*) photocatalytic decomposition of the vapor precursor on the film surface and (*ii*) subsequent diffusion of decomposed elements into the bulk crystal (Figure 5A).[33] Step (*i*) should be the rate-determining step to form an intermixed ternary alloy throughout the film and tune the λ_{PL} by adjusting the photon flux during the photoconversion of constituent elements. The rate of each step can vary dramatically based on the strength of the photocatalytic effect of the host film in decomposing adjacent precursors and the diffusion coefficient of the incorporated elements within the film, determining the overall process.

The PL spectra modulation in $CsPbCl_{3-x}Br_x$ film strongly depends on the type of host film, even under identical illumination conditions. When Br substitutes for Cl in $CsPbCl_3$ using a CH_2Br_2 precursor (Figure 5B), single peaks with continuously varying λ_{PL} from 420 to 523 nm emerge. Conversely, when Cl replaced Br in $CsPbBr_3$ using a CH_2Cl_2 precursor, the PL peak for $CsPbBr_3$ at 520 nm gradually diminishes, while the peak for $CsPbCl_3$ at 420 nm appears (Figure 5C), indicating the formation of segregated phases of $CsPbBr_3$ and $CsPbCl_3$. The differing behaviors in these cases can be attributed to the varying halogen diffusivities in the host films, influenced by atomic vacancies.[34−36] $CsPbBr_3$ has been reported to possess a significantly lower equilibrium vacancy concentration than $CsPbCl_3$, with vacancy formation energies for Schottky defect pairs estimated at 0.35 and 0.42 eV for $CsPbBr_3$ and $CsPbCl_3$, respectively.[34] As a result, the interdiffusion rate of Cl into $CsPbBr_3$ crystallites from the surface is significantly reduced, leading to an abrupt junction (see schematics in Figure 5C). Since intermixed perovskite alloys are more thermodynamically stable than segregated phases,[37,38] Cl will eventually diffuse throughout the $CsPbBr_3$ crystallites. Nevertheless, if the decomposition rate of Cl-containing precursors on the surface exceeds the diffusion rate, the resulting composition profile will be diffusion-limited with an abrupt junction.

For the case of Figure 5B, the relative ratio of substituted Br among all the halogens, X_{Br}, inferred from λ_{PL} is plotted as a function of the photoexcited carrier density, N_{ex} at the surface of the host film (Figure 5D). Assuming the total process limited by step (*i*), we fitted the data to an asymptotic exponential function representing saturated exchange behavior as $1 - e^{-\alpha N_{ex}/d_h}$, where d_h is the areal density of the halogen elements at the surface, and α indicates the photocatalytic efficiency for halogen exchanges (see Supporting Information for details). The deduced α value is close to 2 in the low N_{ex} regime (blue fitted curve), indicating the efficient photo-

https://doi.org/10.1021/acs.nanolett.4c02153
Nano Lett. XXXX, XXX, XXX−XXX

conversion of the dihalide precursor of CH_2Br_2. As the conversion progresses, the halogen conversion rate by decomposing the CH_2Br_2 precursor slows, with the reduced α value of 0.53 (red curve). This slowdown is presumably due to a change in the relative electronic energy levels of the Br-rich $CsPbCl_{3-x}Br_x$ film in the photoexcited states, and the precursor molecules, which govern the charge transfer process essential for photocatalytic conversion.[18,39] Nevertheless, the entire process is constrained by the slower step (*i*), enabling precise modulation of λ_{PL} by controlling the excited UV photon flux to achieve full conversion with X_{Br} approaching 1.

The α value is highly sensitive to the type of precursor as well, affecting the kinetics of the overall process. When iodine was substituted for bromine in $CsPbBr_3$ using an CH_2I_2 precursor, modulation of λ_{PL} from a single peak was observed, indicating the formation of homogeneous $CsPbBr_{3-x}I_x$ alloys (Figure 4D, Figure S3C). Unlike chlorine, which separates phases within the same host film, iodides form a mixed phase because iodine has a faster diffusion rate than chlorine within the $CsPbBr_3$ structure. This is due to their relative bonding strength to lead, with chlorine forming a stronger bond than iodine.[40] In the N_{ex}-dependent X_I data (Figure 5E), the deduced α of 8.4×10^{-3} is more than 2 orders of magnitude lower than that in Figure 5D. This finding aligns with the higher dissociation energy of C-I bonds in the CH_2I_2 precursor than C-Br bonds in the CH_2Br_2 precursor.[41] Thus, the slower step (*i*) could still be the rate-determining step despite the expectedly low Iodine-diffusion rate[41] in the $CsPbBr_3$ film of 2.08×10^{-11} cm^2/s. We note that the diffusivity plays important roles to determine not only the kinetics of halide exchange process, but also the spatial resolution of our technique (Figure S7), and can be engineered by changing the grain structures of host films (refer to the Supporting Information for a detailed discussion).

Our approach to designing semiconductor alloy patterns can be extensively applied across a range of applications. Lead-based halide perovskites are known to be excellent hole and electron conductors,[42,43] allowing for the creation of composition-modulated circuitry that forms various functional multispectral optoelectronic elements. These include wavelength-tunable solid-state light emitters with confined type-I heterostructures, and broadband photodiodes with band-graded junctions. Alloy formation and patterning occur simultaneously through a bottom-up approach, eliminating the need for additional integration steps; thus, the fabrication of complex integrated circuitry is made possible. Furthermore, by using different precursors, this method can be adapted to various semiconductor systems[44] for spatial control of their band gap and/or electrochemical potentials. This strategy is particularly advantageous for designing circuitry with nanomaterial systems,[11,45] where conventional top-down patterning processes are not viable due to structural or chemical instability.

■ ASSOCIATED CONTENT

Supporting Information

The Supporting Information is available free of charge at https://pubs.acs.org/doi/10.1021/acs.nanolett.4c02153.

Preparation of host perovskite films, Fabrication of optical density-gradient photomasks, Single-shot optical lithography for multispectral patterns, Optical characterizations of multispectral patterns, Demonstrations of compressive optical spectroscopy with multivariant emissive films, Estimation of photocatalytic efficiency for halide exchange, α (PDF)

■ AUTHOR INFORMATION

Corresponding Authors

Yong-Young Noh − *Department of Chemical Engineering, Pohang University of Science and Technology (POSTECH), Pohang 37673, Republic of Korea;* orcid.org/0000-0001-7222-2401; Email: yynoh@postech.ac.kr

Cheol-Joo Kim − *Center for Van der Waals Quantum Solids, Institute for Basic Science (IBS), Pohang 37673, Republic of Korea; Department of Chemical Engineering, Pohang University of Science and Technology (POSTECH), Pohang 37673, Republic of Korea;* orcid.org/0000-0002-4312-3866; Email: kimcj@postech.ac.kr

Authors

Hyewon Shim − *Center for Van der Waals Quantum Solids, Institute for Basic Science (IBS), Pohang 37673, Republic of Korea; Department of Chemical Engineering, Pohang University of Science and Technology (POSTECH), Pohang 37673, Republic of Korea*

Geonwoong Park − *Department of Chemical Engineering, Pohang University of Science and Technology (POSTECH), Pohang 37673, Republic of Korea*

Hyunsuk Yun − *Department of Chemistry, POSTECH, Pohang 37673, Republic of Korea*

Sunmin Ryu − *Department of Chemistry, POSTECH, Pohang 37673, Republic of Korea;* orcid.org/0000-0002-6860-6514

Complete contact information is available at: https://pubs.acs.org/10.1021/acs.nanolett.4c02153

Author Contributions

H.-W.S., Y.-Y.N., and C.-J.K. designed the experiments. G.-W.P. synthesized $CsPbBr_3$ samples. H.-W.S. built the optical lithography setup and fabricated multispectral patterns. H.-W.S. and H.-S.Y. conducted PL measurements. H.-W.S. conducted optical data analyses for the demonstration of dispersive optics-free spectroscopy. H.-W.S. and C.-J.K. wrote the manuscript with inputs from all authors.

Funding

This research was supported by the National R&D Program through the National Research Foundation of Korea (NRF) funded by the Ministry of Science and ICT (2020R1A4A1019455, 2020M3D1A1110548, 2023R1A2C2005427) and the Institute for Basic Science (IBS-R034-D1).

Notes

The authors declare no competing financial interest.

■ REFERENCES

(1) Hunt, R. W. G. *The reproduction of colour*; John Wiley & Sons, 2005.

(2) Pattison, P.; Tsao, J.; Brainard, G.; Bugbee, B. LEDs for photons, physiology and food. *Nature* **2018**, *563* (7732), 493−500.

(3) Wetzstein, G.; Ozcan, A.; Gigan, S.; Fan, S.; Englund, D.; Soljačić, M.; Denz, C.; Miller, D. A.; Psaltis, D. Inference in artificial intelligence with deep optics and photonics. *Nature* **2020**, *588* (7836), 39−47.

(4) Fontaine, N. K.; Haramaty, T.; Ryf, R.; Chen, H.; Miron, L.; Pascar, L.; Blau, M.; Frenkel, B.; Wang, L.; Messaddeq, Y.

Heterogeneous space-division multiplexing and joint wavelength switching demonstration. In *Optical Fiber Communication Conference Post Deadline Papers, OSA Technical Digest (online) (Optica Publishing Group, 2015)*, DOI: 10.1364/OFC.2015.Th5C.5.
(5) Richardson, D. J.; Fini, J. M.; Nelson, L. E. Space-division multiplexing in optical fibers. *Nat. photonics* **2013**, *7* (5), 354−362.
(6) Zhao, Y.; Wang, V.; Lien, D.-H.; Javey, A. A generic electroluminescent device for emission from infrared to ultraviolet wavelengths. *Nat. Electron.* **2020**, *3* (10), 612−621.
(7) Nobeshima, T.; Nakakomi, M.; Nakamura, K.; Kobayashi, N. Alternating-current-driven, color-tunable electrochemiluminescent cells. *Adv. Opt. Mater.* **2013**, *1* (2), 144−149.
(8) Wang, V.; Uddin, S. Z.; Park, J.; Javey, A. Highly multicolored light-emitting arrays for compressive spectroscopy. *Sci. Adv.* **2023**, *9* (16), eadg1607.
(9) Yang, Z.; Albrow-Owen, T.; Cui, H.; Alexander-Webber, J.; Gu, F.; Wang, X.; Wu, T.-C.; Zhuge, M.; Williams, C.; Wang, P.; et al. Single-nanowire spectrometers. *Science* **2019**, *365* (6457), 1017−1020.
(10) Bao, J.; Bawendi, M. G. A colloidal quantum dot spectrometer. *Nature* **2015**, *523* (7558), 67−70.
(11) Ning, C.-Z.; Dou, L.; Yang, P. Bandgap engineering in semiconductor alloy nanomaterials with widely tunable compositions. *Nat. Rev. Mater.* **2017**, *2* (12), 1−14.
(12) Hahm, D.; Lim, J.; Kim, H.; Shin, J.-W.; Hwang, S.; Rhee, S.; Chang, J. H.; Yang, J.; Lim, C. H.; Jo, H.; et al. Direct patterning of colloidal quantum dots with adaptable dual-ligand surface. *Nat. Nanotechnol.* **2022**, *17* (9), 952−958.
(13) Yang, J.; Lee, M.; Park, S. Y.; Park, M.; Kim, J.; Sitapure, N.; Hahm, D.; Rhee, S.; Lee, D.; Jo, H.; et al. Nondestructive photopatterning of heavy-metal-free quantum dots. *Adv. Mater.* **2022**, *34* (43), 2205504.
(14) Yang, J.; Hahm, D.; Kim, K.; Rhee, S.; Lee, M.; Kim, S.; Chang, J. H.; Park, H. W.; Lim, J.; Lee, M.; et al. High-resolution patterning of colloidal quantum dots via non-destructive, light-driven ligand crosslinking. *Nat. Commun.* **2020**, *11* (1), 2874.
(15) Sun, K.; Tan, D.; Fang, X.; Xia, X.; Lin, D.; Song, J.; Lin, Y.; Liu, Z.; Gu, M.; Yue, Y.; Qiu, J. Three-dimensional direct lithography of stable perovskite nanocrystals in glass. *Science* **2022**, *375* (6578), 307−310.
(16) Sun, L.; Wang, R.; Wang, W.; Wang, S.; Yang, X.; Dai, J. Excitonic optical properties of cesium trifluoroacetate induced $CsPbBr_3$ thin film with anti-solvent treatment. *Opt. Mater.* **2020**, *106*, 110005.
(17) Wong, Y. C.; Wu, W. B.; Wang, T.; Ng, J. D. A.; Khoo, K. H.; Wu, J.; Tan, Z. K. Color patterning of luminescent perovskites via light-mediated halide exchange with haloalkanes. *Adv. Mater.* **2019**, *31* (24), 1901247.
(18) Parobek, D.; Dong, Y.; Qiao, T.; Rossi, D.; Son, D. H. Photoinduced anion exchange in cesium lead halide perovskite nanocrystals. *J. Am. Chem. Soc.* **2017**, *139* (12), 4358−4361.
(19) Ghaithan, H. M.; Qaid, S. M.; Alahmed, Z. A.; Hezam, M.; Lyras, A.; Amer, M.; Aldwayyan, A. S. Anion substitution effects on the structural, electronic, and optical properties of inorganic $CsPb(I_{1-x}Br_x)_3$ and $CsPb(Br_{1-x}Cl_x)_3$ perovskites: Theoretical and experimental approaches. *J. Phys. Chem. C* **2021**, *125* (1), 886−897.
(20) Wang, Y.; Jia, C.; Fan, Z.; Lin, Z.; Lee, S.-J.; Atallah, T. L.; Caram, J. R.; Huang, Y.; Duan, X. Large-area synthesis and patterning of all-inorganic lead halide perovskite thin films and heterostructures. *Nano Lett.* **2021**, *21* (3), 1454−1460.
(21) Dou, L.; Lai, M.; Kley, C. S.; Yang, Y.; Bischak, C. G.; Zhang, D.; Eaton, S. W.; Ginsberg, N. S.; Yang, P. Spatially resolved multicolor $CsPbX_3$ nanowire heterojunctions via anion exchange. *PNAS* **2017**, *114* (28), 7216−7221.
(22) Wyszecki, G. Concepts and methods, quantitative data and formulae. *Color Science* **1982**, 130−175.
(23) Oh, J.; Baek, D.; Lee, T. K.; Kang, D.; Hwang, H.; Go, E. M.; Jeon, I.; You, Y.; Son, C.; Kim, D.; et al. Dynamic multimodal holograms of conjugated organogels via dithering mask lithography. *Nat. Mater.* **2021**, *20* (3), 385−394.
(24) Lee, J. S.; Park, J. Y.; Kim, Y. H.; Jeon, S.; Ouellette, O.; Sargent, E. H.; Kim, D. H.; Hyun, J. K. Ultrahigh resolution and color gamut with scattering-reducing transmissive pixels. *Nat. Commun.* **2019**, *10* (1), 4782.
(25) Ahn, J.; Jeon, S.; Woo, H. K.; Bang, J.; Lee, Y. M.; Neuhaus, S. J.; Lee, W. S.; Park, T.; Lee, S. Y.; Jung, B. K.; et al. Ink-lithography for property engineering and patterning of nanocrystal thin films. *ACS nano* **2021**, *15* (10), 15667−15675.
(26) Lin, S.; Tang, Y.; Kang, W.; Bisoyi, H. K.; Guo, J.; Li, Q. Photo-triggered full-color circularly polarized luminescence based on photonic capsules for multilevel information encryption. *Nat. Commun.* **2023**, *14* (1), 3005.
(27) Feng, P.; Yang, X.; Feng, X.; Zhao, G.; Li, X.; Cao, J.; Tang, Y.; Yan, C.-H. Highly stable perovskite quantum dots modified by europium complex for dual-responsive optical encoding. *ACS nano* **2021**, *15* (4), 6266−6275.
(28) Wang, Z.; Shen, J.; Xu, B.; Jiang, Q.; Ming, S.; Yan, L.; Gao, Z.; Wang, X.; Zhu, C.; Meng, X. Thermally driven amorphous-crystalline phase transition of carbonized polymer dots for multicolor room-temperature phosphorescence. *Adv. Opt. Mater.* **2021**, *9* (16), 2100421.
(29) Chen, J.; Zeng, Y.; Sun, R.; Zhang, W.; Huang, Y.; Zheng, J.; Chi, Y. Hydrochromic perovskite system with reversible blue-green color for advanced anti-counterfeiting. *Small* **2023**, *19*, 2301010.
(30) Li, L.-Y.; Li, D.; Dong, X.; Tan, Q.-W.; Wang, X.-L.; Wang, Y.-Z.; Song, F. A confined self-assembly approach towards chiral photonic materials with circularly polarized structural colors for information storage and encryption. *Chem. Eng. J.* **2024**, *479*, 147669.
(31) Xue, Y.; Lai, X.; Wang, L.; Shi, H.; Liu, G.; Liu, X.; Chen, X. A stimuli-responsive hydrogel for reversible information storage, encryption and decryption. *J. Colloid Interface Sci.* **2024**, *662*, 231−241.
(32) Austen, K. The trouble with wearables. *Nature* **2015**, *525* (7567), 22.
(33) Zhang, Y.; Lu, D.; Gao, M.; Lai, M.; Lin, J.; Lei, T.; Lin, Z.; Quan, L. N.; Yang, P. Quantitative imaging of anion exchange kinetics in halide perovskites. *PNAS* **2019**, *116* (26), 12648−12653.
(34) Lai, M.; Obliger, A.; Lu, D.; Kley, C. S.; Bischak, C. G.; Kong, Q.; Lei, T.; Dou, L.; Ginsberg, N. S.; Limmer, D. T.; et al. Intrinsic anion diffusivity in lead halide perovskites is facilitated by a soft lattice. *PNAS* **2018**, *115* (47), 11929−11934.
(35) Shahjahan, M.; Yuyama, K. i.; Okamoto, T.; Biju, V. Heterojunction perovskite microrods prepared by remote-controlled vacancy filling and halide exchange. *Adv. Mater. Technol.* **2021**, *6* (2), 2000934.
(36) Yoon, S. J.; Kuno, M.; Kamat, P. V. Shift happens. How halide ion defects influence photoinduced segregation in mixed halide perovskites. *ACS Energy Lett.* **2017**, *2* (7), 1507−1514.
(37) Bischak, C. G.; Hetherington, C. L.; Wu, H.; Aloni, S.; Ogletree, D. F.; Limmer, D. T.; Ginsberg, N. S. Origin of reversible photoinduced phase separation in hybrid perovskites. *Nano Lett.* **2017**, *17* (2), 1028−1033.
(38) Cho, J.; Kamat, P. V. Photoinduced phase segregation in mixed halide perovskites: thermodynamic and kinetic aspects of Cl−Br segregation. *Adv. Opt. Mater.* **2021**, *9* (18), 2001440.
(39) Gomathi Devi, L.; Mohan Reddy, K. Photocatalytic performance of silver TiO_2: Role of electronic energy levels. *Appl. Surf. Sci.* **2011**, *257* (15), 6821−6828.
(40) Koscher, B. A.; Bronstein, N. D.; Olshansky, J. H.; Bekenstein, Y.; Alivisatos, A. P. Surface-vs diffusion-limited mechanisms of anion exchange in $CsPbBr_3$ nanocrystal cubes revealed through kinetic studies. *J. Am. Chem. Soc.* **2016**, *138* (37), 12065−12068.
(41) Chen, W.; Li, W.; Gan, Z.; Cheng, Y. B.; Jia, B.; Wen, X. (2019). Long-distance ionic diffusion in cesium lead mixed halide perovskite induced by focused illumination. *Chem. Mater.* **2019**, *31* (21), 9049−9056.

https://doi.org/10.1021/acs.nanolett.4c02153
Nano Lett. XXXX, XXX, XXX−XXX

(42) Liu, A.; Zhu, H.; Bai, S.; Reo, Y.; Caironi, M.; Petrozza, A.; Dou, L.; Noh, Y.-Y. High-performance metal halide perovskite transistors. *Nat. Electron.* **2023**, *6* (8), 559−571.
(43) Li, Z.; Zhang, B.; Zhang, Z.; Bunzli, J.-C.; Mohd Yusoff, A. R. b.; Noh, Y.-Y.; Gao, P. Vitamin needed: Lanthanides in optoelectronic applications of metal halide perovskites. *Mater. Sci. Eng.: R: Rep.* **2023**, *152*, 100710.
(44) Seo, S.-Y.; Moon, G.; Okello, O. F.; Park, M. Y.; Han, C.; Cha, S.; Choi, H.; Yeom, H. W.; Choi, S.-Y.; Park, J.; et al. Reconfigurable photo-induced doping of two-dimensional van der Waals semiconductors using different photon energies. *Nat. Electron.* **2021**, *4* (1), 38−44.
(45) Park, J.-H.; Reo, Y.; Jung, J.-H.; Kim, T.; Park, T.; Noh, Y.-Y.; Kim, C.-J. Reduction of Hole Carriers by van der Waals Contact for Enhanced Photoluminescence Quantum Yield in Two-Dimensional Tin Halide Perovskite. *ACS Energy Lett.* **2023**, *8* (8), 3536−3544.

https://doi.org/10.1021/acs.nanolett.4c02153
Nano Lett. XXXX, XXX, XXX−XXX